Wide Field Imaging

Prashansa Gupta

A dissertation submitted for the partial fulfillment of BS-MS Dual Degree in Science

Indian Institute of Science Education and Research Mohali

April 2016

Certificate of Examination

This is to certify that the dissertation titled **'Wide Field Imaging'** submitted by **Ms Prashansa Gupta** (Registration No MS11021) for the partial fulfillment of BS-MS Dual Degree program of the Institute has been examined by the thesis committee duly appointed by the Institute. The committee finds the work done by the candidate satisfactory and recommends that the report be accepted.

Prof Jasjeet Singh Bagla Dr Harvinder Kaur Jassal Dr Manimala Mitra

(Supervisor)

Dated: April 22, 2016

Declaration

The work presented in this presentation has been carried out by me under the guidance of Prof Jasjeet Singh Bagla at the Indian Institute of Science Education and Research Mohali. This work has not been submitted in part or in full for a degree, a diploma or a fellowship to any other university or an institute. Whenever contributions of other are involved every effort is made to indicate this clearly with due acknowledgment of collaborative research and discussions. This thesis is a bonafide record of original work done by me and all sources listed within have been detailed in the bibliography.

Prashansa Gupta

(Candidate)

Dated: April 22, 2016

In my capacity as the supervisor of the candidate's project work, I certify that the above statements by the candidate are true to the best of my knowledge.

Prof Jasjeet Singh Bagla

(Supervisor)

Acknowledgements

I wish to first of all acknowledge, with gratitude, the immense support Prof Jasjeet Singh Bagla has provided me, not just for this project but during all the five years of my undergraduate study at IISER Mohali. I had come to him with an inclination towards astronomy, and he bolstered that into a full fledged career choice. His unflinching optimism towards worst of the things has brought me out of my lows. I appreciate the way he helps, it is just enough to get things started instead of him not giving any idea or worst still, spoonfeeding! I admire his honesty, and the unfaltering effort he puts into his work, and I wish to imbibe such qualities. He has supported me through my decisions and guided me when it was required. I am indebted to him for believing in my sincerity without which I would not be where I am today.

I wish to thank Dr Harvinder Kaur Jassal for her constant encouragement throughout this work. Even though she was not directly involved with it, she has shown her support through her words and faith, and through healthy discussions during weekly meetings. I also wish to thank Dr Manimala Mitra, for whatever little times we have interacted.

I owe a great debt to all the faculty with whom I have had correspondence all throughout these five years. I extend a heartfelt thanks to Prof Sudeshna Sinha, for always being available and never refusing to help and for her kind words of encouragement that have kept me moving forward. Many thanks are in order for Dr Abhishek Chaudhari who always kept a check on me during and after the courses, who is a brilliant teacher and whose infectious enthusiasm towards science has always encouraged me to do better. My frequent interactions with Dr N. G. Prasad first during his excellent course on evolution and then on general issues of campus life, made me understand the importance of humility and I thank him for

being such a mentor.

I would like to thank Prof Kapil Paranjape, Dr Amit Kulsreshtha, Dr Purnananda Guptasarma, Dr Dipanjan Chakraborty, Dr Arvind, Dr Sanjay Mandal, Prof C S Aulakh for all good natured interactions and advice they have given and for taking care of me.

I have made friends for life here and I wish to thank them for being who they are. I am truly grateful to Atul Singh Arora for being a splendid study partner, for his humility and humour and for providing me his unrestricted attention in situations where I needed his help, be it programming issues or personal ones. I am indebted to Manisha for all the good and the bad times we have shared together that have made our friendship stronger each day. I am thankful to Ritu Roy Chowdhury for being such a brilliant person guiding me to the correct path with her humour, and to Vivek Sagar for being such a good companion. I owe a lot of good memories to Manu J., Kishor Bharti, Abhinay Vardhan, Shwetha S., Yosman Bapat Dhar, Srijit Mukherjee, Saumya and Arjit Kant Gupta without whom my stay and this work would not be complete.

I dedicate this work to my parents, to whom I will be indebted to always. I cannot thank them enough. Their incessant support, faith and encouragement is invaluable, and their teachings have helped me move through life. I thank my loving sister Shailja for being a friend and being a healthy & happy influence on my life.

Abstract

Interferometry has been used in radio astronomy for quite some time now, becoming an essential technique that makes high resolution imaging possible with radio telescopes. The existent mathematical framework for this relies heavily on the assumption of a small field of view and co-planarity of the array, and, a quasi-monochromatic regime in the form of the van Cittert Zernike theorem. Technological advances, however, have now made it possible to study large portions of the sky with a broader bandwidth, giving rise to the need to revisit the mathematics. There is a related complexity introduced by SKA, LOFAR like non-coplanar arrays, the so called w-term. Some of these issues can be tackled by using non-cartesian basis functions, for example, spherical harmonics. The aim of this thesis is to study generalizations of the existing methodologies to reduce or even remove the restrictive assumptions, taking the examples of the GMRT, OWFA, MWA telescopes.

List of Figures

Contents

Chapter 1

Introduction

A fleeting glance over the night sky could be sufficient to tell the casual observer that the universe is filled with bright objects. An admirer of the night sky would be able to spot out differences in brightness and probably sizes of these objects. The astronomer, however, will be able to precisely elaborate on the differences among them, and point out the usual classification of stars, planets, satellites, galaxies, clusters and so on. The astronomer's eyes are aided by the telescope, that has a greater resolving power than the naked eye.

Over about a hundred years, the telescopes have become more complex. From simply supported-on-a-stand-reflectors to large dishes maneuvered by computers to space observatories and unmanned missions.

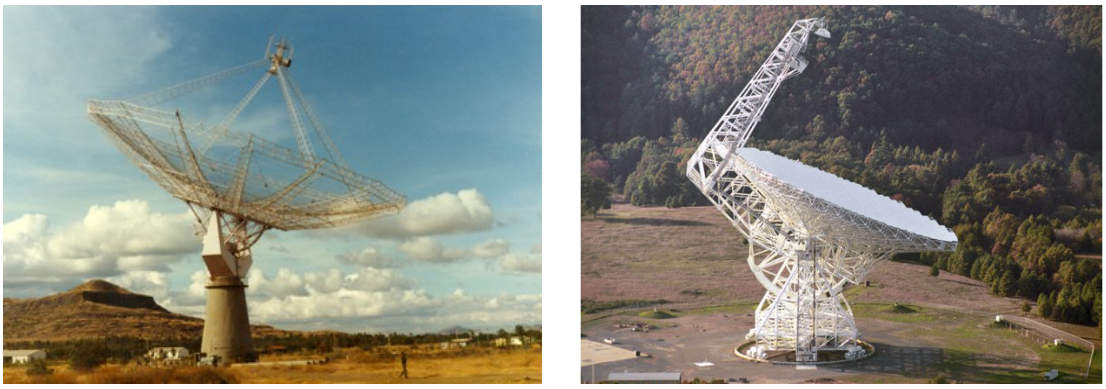

Figure 1.1: Left: The Giant Meterwave Radio Telescope in India[4], Right: The Green Bank Telescope in West Virginia, USA. [11]

The first advancement was the replacement of the eye by a photographic plate as the detector. These plates stored the images of the sources for later review and

comparison, reducing the dependency on the human eye and memory.

When the optical regime of the electromagnetic spectrum became limited, other frequencies started becoming useful. Last few decades have also seen the emergence of neutrino based astronomy, and very recently gravitational waves have also proved to be very useful probes of the universe. Since our eyes could only see the visible light, such other possibilities had remained unexplored. It was only through telescopes that we were able to charter the unknown regions, and eventually found a wealth of information hidden.

A huge part of the electromagnetic spectrum is labeled as the radio regime, beginning from micrometer to few kilometer long wavelengths. Fortunately, the atmosphere is transparent in most of this region, which makes observations of radio sources ideal.

The telescopes may be simply pointed at the source of choice and analyzed for its emission. Figure 1.1 shows typical radio single dishes But in order to get a detailed image of the region, it might be scanned multiple times and different parts pieced together.

Single dish telescopes, due to their finite size, are limited in their resolving power. As we will see, this restriction is more pronounced in the radio regime. Astronomers have come up with the technique of interferometry wherein not one but a number of antennas are used to synthesize one image. These telescopes are to be arranged in patterns that optimize the resolving power against the time required for image synthesis. Figure 1.2 shows some examples.

Figure 1.2: Left: The Very Large Array in New Mexico [12], Right: The Giant Meterwave Radio Telescope in India [4]

Naively, one would expect the rotation and revolution of the Earth to be a bane for such measurements since the sources of interest will never be fixed at one point for numerous observations! But astronomers have worked their way out and have indeed usefully employed this phenomenon.

Astronomy also has an elaborate set of coordinate systems in place. As we will see, constellations, orbits of the Sun and the Earth help define an imaginary celestial sphere. Latitudes and Longitudes, similar to that for the Earth, are used to refer to the source of interest uniquely.

The antennas on the Earth coupled with the electronic backend record the incoming electromagnetic waves in the form of voltage changes called visibilities. Converting them back to the original brightness distribution on the sky requires processing and as will be discussed, it is often limited by the antenna's own response function.

While the study of small regions of sky and in the limit where objects far away can be approximated to lie in a plane instead of three dimensional spaces, we are easily able to image the sky. We will see that, as our regions of interest grow wider, this process becomes tedious and various approximations are then applied.

In this work, we begin by understanding what do our antennas actually measure when pointed towards the source of interest and how do we represent these 'signals' mathematically. We then move on to describing the technique of interferometry introduced above, and see how movement of the Earth is applied. We study the current method of imaging by relating the actual brightness of the sources with the visibilities. We move on to imaging in wider regions of the sky and try to obtain relations simpler than the usual ones used.

Chapter 2

Signals and Noise

A record of electric field $E(t)$ received at any point on the Earth from a source, in our case a radio source, is called a 'signal'. This emanates from a large object that has many independently radiating parts that differ in frequencies, distance from the observation point etc. This implies it can be called random in character. As observed, the statistical properties do uphold this assumption, as all of them are consistent with a model where different frequencies have completely unrelated phases and each phase varies randomly from 0 to 2π. These 'signals' are thus 'time stationary gaussian noise', where noise refers to its random character. The systematic variation of the strength or amplitude squared of different frequencies ω is called the power spectrum $S(\omega)$. 'Noise' is the unwanted disturbance which is added to the signal being received unavoidably. Ofcourse, just like the 'signals', it is also the 'time stationary gaussian' type.

2.1 Signals

Consider a plane wavefront from a distant point source falling on Earth. If the energy per unit frequency passing through an area of one square meter held perpendicular to the line of sight to the source is $10^{-26}W$ then the source is said to have brightness of one Jansky. Thus one Jansky is 10^{-26} watts per unit area per unit frequency. For an extended source, one also has to add another qualification of per unit solid angle since there is no unique direction to hold the square meter.

Often, radio astronomers employ temperature units for sky brightness.

Consider a black body at temperature T, its radiation is described by the Planck spectrum

$$B(\nu) = \frac{2h\nu^3}{c^2} \frac{1}{e^{h\nu/kT} - 1} \quad \text{W/m}^2 \text{ Hz sr} \tag{2.1}$$

For a typical radio frequency of, say, 1000 MHz, $h\nu/k = 0.048$, hence in the Rayleigh - Jeans limit of $T >> h\nu/kT$ or $\nu << kT/h$,

$$B(\nu) \approx \frac{2kT}{\lambda^2} \tag{2.2}$$

is valid across most of the radio spectrum. Brightness temperature of an extended source is defined as

$$T_B = \frac{\lambda^2}{2k} B(\nu) \tag{2.3}$$

It is important to note that there is no relation between the physical and the brightness temperatures of the source.

Consider a resistor kept in thermal bath at temperature T, where the electron's random thermal motion causes current to flow in the resistor. Eventhough the average current is zero, the power is not since it depends on the square of the current. In the radio regime, the power per unit frequency is well approximated by the Nyquist Formula as

$$P = kT \tag{2.4}$$

where k is the Boltzmann constant. Setting an analogy, if power P per unit frequency is available at an antenna's terminals the antenna is defined to have an antenna temperature of

$$T_A = \frac{P}{k} \tag{2.5}$$

Again, this antenna temperature is different from the physical temperature of the antenna. Similarly, the total power available at the terminals of a radio telescope is defined as the system temperature

$$T_{sys} = \frac{\text{Total power referred to receiver inputs}}{k} \tag{2.6}$$

2.2 Noise

When looking at a region of the sky without any sources, system temperature gives a measure of total random noise in the system, hence it is desirable to make it as low as possible. Noise from various subsystems is uncorrelated and adds up linearly. Thus system temperature can be written as

$$T_{sys} = T_{sky} + T_{spill} + T_{loss} + T_{rec} \tag{2.7}$$

T_{sky} is the contribution from the background sky brightness for example the cosmic background radiation which always contributes 3K.
Often the feed antenna also picks up added noise in the form of stray radiation from the ground, contributing to the T_{spill}.
Lossy elements in the path of the feed contribute to T_{loss}, since due to Kirchoff's laws good absorbers are also good emitters. Also the ratio of emission to absorption in thermodynamic equilibrium is given by Planck spectrum at the absorber's physical temperature.Thus. almost all of the elements between the feed and the amplifier are cooled.
The receiver adds noise to the system contributed in the T_{rec}.

Chapter 3

Mathematical Background

We had asserted previously that the signals and noise were of the 'time stationary gaussian' variety. Time stationary means that the signal in one interval is statistically indistinguishable from that in another equal duration but time shifted interval. Just like all probabilistic statements, its validity can only be made more probable by repeated experimentation but not precisely checked, for example, by looking at the probability distribution of the signal amplitude. Take a stretch of the signal, from 0 to time T, say, and make a histogram of N equally spaced values $E(t_i)$ where i goes from 1 to N. The property of time stationarity then says that this histogram will turn out to be statistically the same to that when one had chosen an interval t to $t+T$ for any t. The calculable errors decrease with increasing N. Secondly, as N tends to infinity, random phase superposition of many frequencies makes this histogram tend to a gaussian with zero mean.

3.1 Weiner Khinchin Theorem

From the Fourier theory, we can write

$$E(t) \equiv \sum a_n \cos \omega_n t + b_n \sin \omega_n t = \sum r_n \cos(\omega_n t + \phi_n)$$

where

$$\omega_n = \frac{2\pi}{T}; \quad r_n = \sqrt{a_n x^2 + b^2{}_n} \quad \text{and} \quad \tan \phi_n = \frac{-b_n}{a_n}$$

In the limit of T going to large values, the frequencies form a closely spaced set. The autocorrelation

$$C(\tau) = \langle E(t)E(t+\tau)\rangle$$
$$= \langle \sum_n r_n \cos(\omega_n t + \phi_n) \sum_m r_m \cos(\omega_m (t+\tau) + \phi_m)\rangle$$

On the right hand side, the phases ϕ_k vary independently from 0 to 2π, which implies that only terms with $m = n$ survive giving

$$C(\tau) = \sum \frac{1}{2} r_n^2 \cos \omega_n \tau$$

This autocorrelation is time stationary, since it is independent of time t. For zero delay,

$$C(0) = \langle (t)^2 \rangle = \sum \frac{1}{2} r_n^2$$

which is the variance of the signal. The number of frequencies in a given bandwidth $\Delta\omega$ goes as $\frac{\Delta\omega}{2\pi/T}$. In the limit $T \to \infty$, this number blows up.

For $C(\tau)$ to have a well defined behavior in this limit, then r_n^2 will have to scale inversely with T so that the weight of the terms being added decreases and the sum reaches a limiting value . Since the number of r_n's even in a small interval $\Delta\omega$ blows up, their combined effect becomes more important than their individual one which motivates the following definition for $T \to \infty$

$$\sum_{\omega < \omega_n < \omega + \Delta\omega} \frac{r_n^2}{2} = 2S(\omega)\Delta\omega$$

$S(\omega)$ is called the *power spectrum* since, $2S(\omega)\Delta\omega$ is the contribution to the variance $\langle E^2(t)\rangle$ in the interval ω to $\omega + \Delta\omega$. Thus

$$C(\tau) = \int_0^\infty 2S(\omega) \cos \omega\tau d\omega$$

Define $S(-\omega) = S(\omega)$ and we obtain

$$C(\tau) = \int_{-\infty}^{+\infty} S(\omega) e^{-i\omega\tau} d\omega$$

This equation represents the *Weiner Khinchin Theorem* which states that the autocorrelation function is the Fourier transform of the power spectrum. In terms of frequency

$$C(\tau) = \int_{-\infty}^{+\infty} P(\nu) e^{-2\pi i\nu\tau} d\nu$$

Since we did not make use of the fact that the ϕ's are independent, this theorem is valid for all Gaussian as well as Non Gaussian processes.

We can, in principle, perform two different kinds of experiments to measure $C(\tau)$ and $S(\omega)$. Either record samples of voltage in the time domain and calculate averages of lagged products to obtain C or pass the signal through a filter in the frequency domain admitting a narrow band of frequencies around ω and measure the average power that gets through.

As an example, consider a flat band power spectrum between $\nu_o - B/2$ and $\nu_o + B/2$. Its autocorrelation function, for $P(\nu) = K$ say,

$$\begin{aligned} C(\tau) &= 2K \int_0^{\infty} \cos(2\pi\nu\tau) d\nu \\ &= 2KB \cos(2\pi\nu_o\tau) \left(\frac{sin(\pi B\tau)}{\pi B\tau} \right) \end{aligned}$$

The factor $2KB$ is the value at $\tau = 0$, which implies it is the total power, while the cos factor is an oscillation at the center frequency . If $B \ll \nu_o$, then the sinc factor is close to one, for values of τ extending over say $1/4B$, which is still many cycles of the center frequency. This then approaches the limiting case of a single sinusoidal wave whose autocorrelation is sinusoidal.

NYQUIST SAMPLING INTERVAL Another example is the case where the band extends from 0 to B, when the center frequency is $\nu_o = B/2$ which is the so called

'Baseband'. The autocorrelation is

$$C(\tau) = 2KB\left(\frac{\sin 2\pi\tau B}{2\pi\tau B}\right)$$

The correlation between a pair of voltages measured at an interval of $1/2B$ or any multiple is zero. Thus, clearly, a set of samples measured at this interval would be statistically independent since correlations between any pair will vanish. This is the *Nyquist Sampling Interval*. This is the minimum number of measurements which would have to be made to reproduce the signal.

3.2 Shannon Sampling Theorem

It is a general property of a band limited signal i.e. the signal with zero power outside a bandwidth B, that a set of samples separated by $1/2B$ is sufficient to reconstruct the signal.
Count the number of Fourier coefficients: we have 'a' and 'b' or 'r' and 'ϕ' describing each ω_n. Thus the number of parameters defining the signal is twice the number of frequencies. Hence, the number of real values needed to specify our signal for a time T is

$$2\frac{\Delta\omega}{2\pi/T} = 2\left(\frac{\Delta\omega}{2\pi}\right)T = 2BT$$

which gives the $rate = 2B$ at which real numbers need to be measured to keep pace with signal called the Nyquist Sampling Interval. The Shannon criterion is two samples per cycle of the maximum frequency difference present.

SKETCH PROOF: We begin with a band limited signal $E_r(n/2B)$ being sampled at the Nyquist rate. We employ Whitaker's interpolation formula to construct a continuous signal $E_c(t)$ from these samples as

$$E_c(t) = \sum_n E_r(n/2B)\mathrm{sinc}(2\pi B(t - \frac{n}{2B}))$$

where each sinc function is so chosen, so that they give unity at one sample point and zero at others which implies that E_c is guaranteed to agree with $E_r(t)$ samples. It is also band limited and has the same Fourier coefficients . In the end therefore, we have been able to reconstruct successfully a band limited function from its Nyquist samples.

3.3 Cross Correlations

So far, our signals, after entering the antenna, have been a function of time only. But electric fields, before entering the antenna, are a function of both space and time. In this view, we can obtain a delayed version of the same by moving along the direction to the source, the longitudinal direction. Thus, the frequency content is obtained by Fourier transforming a longitudinal spatial correlation. The spatial correlations transverse to the direction of propagation carry information on the angular power spectrum of the signal i.e. energy as a function of direction in sky. This is actually a generalisation of the Weiner Khinchin theorem to spatial correlations of a complex electric field which is a sum of waves propagating in many different directions, formally the van Cittert Zernike theorem.

As one can see, we are now multiplying and averaging signals coming from different antennas and is thus appropriately called 'cross correlation function'. Now, if the signal at the observer's plane is E(r), then the spatial correlation function is defined as

$$V(x) = \langle E(r)E^*(r+x)\rangle \tag{3.1}$$

The function V is referred to as the visibility function or visibility. Strictly speaking, the angular brackets imply ensemble averaging. For typical radio receivers, bandwidths are of the order of a few MHz, i.e. typically $\frac{\Delta\omega}{\omega} \sim 0.1$ the coherence time then is around microseconds. This means that in a few seconds time, one get several million independent samples to average on. Thus, practically, one is averaging over time and assuming that both ensemble and time averaging are equivalent.

Chapter 4

Aperture Synthesis

The Rayleigh criterion states that the angular resolution of a telescope or a microscope is ultimately diffraction limited and is given as

$$\theta \sim \frac{\lambda}{D} \tag{4.1}$$

where D is the size of the aperture and λ is the wavelength at which the observations are made. In the radio regime, the wavelengths are as long as a metre, so even though the aperture sizes are large, the resolution remains limited. For comparison, human eye has a diffraction limit of $20''$, optical telescopes typically have limits of $0.1''$, but even the largest radio telescopes ($\sim 100m$) have angular resolution of only $\sim 30'$ at one metre wavelength!

The need to achieve higher resolutions, without having to increase the antenna sizes led to the formulation of the technique of *Aperture Synthesis* based on interferometry. This involves use of 'antenna arrays', which along with increasing the effective resolution also increase the total collecting area. But on the downside, this collection of several distinct antenna elements arranged in a particular configuration, usually produces an unfilled aperture, which means that we do not have observations at some points! These array elements could range from fixed dipoles to steerable parabolic reflector antennas. The output from different elements can be combined in different ways to obtain different quantities. The outputs if combined with different phase shifts to yield a single total power gives a *'phased array'*, while if multiplied in pairs and processed to obtain a sky brightness distribution

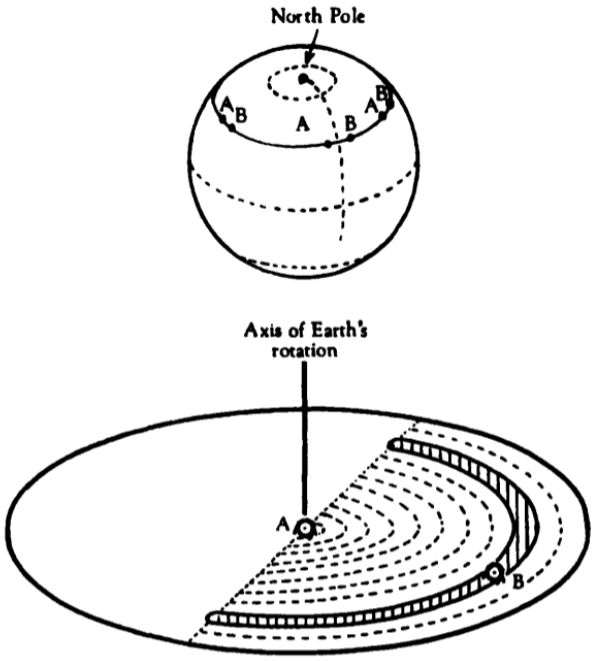

Figure 4.1: The use of rotation of Earth for synthesis mapping. Antennas A and B separated on a East West baseline. [1]

gives a *'correlator array'* or simply an *'interferometer'*.

As we will see, the spatial correlation of electric field observed by different telescopes is related to the source brightness distribution on the sky, and is typically a Fourier Transform relationship. Correlation of voltages from any two radio antennas then allows the measurement of a single Fourier component of the source brightness distribution. Given sufficient number of measurements, the brightness distribution can be obtained by Fourier inversion.

Since the radio sky does not usually vary, it is not necessary to measure all the Fourier components simultaneously. Thus one can imagine measuring all the required Fourier components using just two antennas, by moving one antenna from place to place, gradually building up all the required Fourier components and using them to image the source. In practice however, it is much more useful to employ the rotation of the Earth for 'moving' the antenna around. As seen from the distant cosmic source, the baseline vectors change continuously as the Earth

rotates, changing the Fourier components continuously. If there are N antennas, then at any given instant ${}^{N}C_2$ Fourier components are being measured. Figure 4.1 shows two antennas separated on a East West baseline. All the possible spacings, from the origin to the outermost elliptical boundary of the lower diagram can be taken care of by just varying the distance between the two antennas and observing for 12 h for each configuration. Only 12 h will be required since for the other 12 h the spacings are identical but only the positions of the antennas are interchanged.

The array configuration has a large influence on the kind of sources that can be imaged. From the inverse relationship of Fourier conjugate variables, it follows that short baselines are sensitive to large angular structures, longer baselines sensitive to fine scale structure. The GMRT. for example, has three fourteen km long arms and a densely packed core of one square km, thus gives a combination of long and short spacings amounting to considerable flexibility in the kind of sources that can be imaged. Arrays like the VLA, have their antennas mounted on rails giving even more flexibility!

Chapter 5

Interferometers

5.1 Phase Switching Interferometer

A source in space continously emits signals. Some of the early interferometer receiver systems produced output by adding and squaring the total voltage obtained. Issue with such a methodology was that this output also had additions from other sources which contributed to noise power. These could be the galactic background radiation, thermal noise from the ground or the noise generated in the amplifiers. In general, the signal from the source is several orders of magnitude weaker than that from the noise!

One of the most important breakthroughs in radio interferometery was made by Ryle in 1952 [10] when he introduced *phase switching* mechanism which removed noise and kept only the fringe oscillations.

If the two signal voltages are V_1 and V_2 from antenna 1 and 2 respectively, then addition and squaring yields $(V_1 + V_2)^2$. The phase switching mechanism reverses the second signal periodically, which implies the output now oscillates between $(V_1 + V_2)^2$ and $(V_1 - V_2)^2$. The frequency of this switching is few tens of Hertz, and a synchronized detector takes the difference of these two. As expected, this is proportional to the product of the two voltages $V_1 V_2$.

Thus the output is the time average of the product of these two signals, that is to say it is proportional to the cross correlation of the two signals. The circuitry which performs these tasks of multiplication and time averaging is known as the *correlator*.

5.2 Two element interferometer

Assume a point source in the sky which we would like to observe. Consider two antennas on Earth standing in the East-West direction, separated by a distance D, called the baseline. Under the *far field approximation*, this cosmic source is assumed to be sufficiently distant so that the incident wavefront can be considered to be a plane. One also would like to consider monochromaticity, or single frequency light.

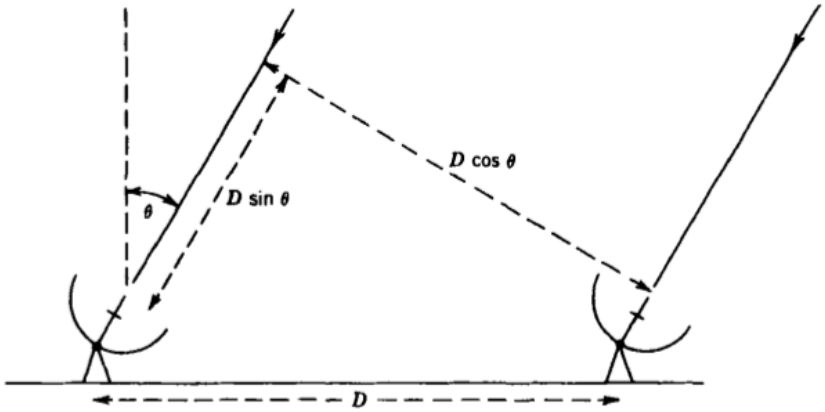

Figure 5.1: Geometry of an elementary interferometer. [3]

If the wavefront from the source reaches the telescope on the right at time t_1, then it reaches the other at time $t_2 = t_1 + \tau_g$, where $t_g = (D/c)\sin\theta$. This τ_g is called the *geometric delay*. The output is then

$$\begin{aligned} F &= 2\sin 2\pi\nu t \sin 2\pi\nu(t-\tau_g) \\ &= \cos 2\pi\nu\tau_g - \cos 4\pi\nu t \cos 2\pi\nu\tau_g - \sin 4\pi\nu t \sin 2\pi\nu\tau_g \end{aligned}$$

The variation of θ is equal to the Earth's rotational velocity of the order of 10^{-4} rad/s. Since D cannot be greater than 10^7m for terrestrial baselines, the rate of variation of $\nu\tau_g$ is smaller than that of νt by atleast six orders of magnitude. The more rapidly varying functions are filtered out, leaving behind the fringe function

$$F = \cos 2\pi\nu\tau_g = \cos\left(\frac{2\pi Dl}{\lambda}\right)$$

where $l = \sin\theta$. As the Earth rotates, θ varies, generating quasisinusoidal fringes at the correlator.

Next, we consider two Fourier components of the signal at frequencies ν_1 and ν_2 instead of one. Since they are statistically independent, the output is then a linear sum of the responses to each component. Hence the output will have F_1 and F_2 as components, and both will have distinct periods at any given θ. This difference in periods give rise to interference in F_1 and F_2, which means that the fringe maxima will have superimposed on them a modulation function depending on θ.

Thus, in the case of a continous band of frequencies, the output is

$$\begin{aligned} F(l) &= \frac{1}{\Delta\nu}\int_{\nu_o-\Delta\nu/2}^{\nu_o+\Delta\nu/2}\cos\left(\frac{2\pi Dl\nu}{c}\right) \\ &= \cos\left(\frac{2\pi lD\nu_o}{c}\right)\frac{\sin(\pi Dl\Delta\nu/c)}{\pi Dl\Delta\nu/c} \end{aligned}$$

where the signals at the correlator are of uniform power spectral density over a bandwidth of $\Delta\nu$. We see that the fringe pattern has an envelope of a sinc function.

This is an example of a general result that in the case of uniform power spectral density at the antennas the envelope of the fringe pattern is the Fourier transform of the instrumental frequency response.

Chapter 6

Antenna Patterns

6.1 Description

How efficient is our antenna in collecting radio waves incident on it? We describe effective aperture as

$$A_e(\theta, \phi) = \frac{\text{Power density available at antenna terminals}}{\text{Flux density of waves incident on antenna}} \tag{6.1}$$

units being

$$\frac{W/Hz}{W/m^2Hz} = m^2 \tag{6.2}$$

This is a function of the angular coordinates since the antenna 'sees' better in some directions than in others.

This describes the *power pattern* of the antenna, usually normalized to unity at the maximum as

$$P(\theta, \phi) = \frac{A_e(\theta, \phi)}{A_e{}^{\max}} \tag{6.3}$$

Another function is the *field pattern* $f(\theta, \phi)$ which is described in the same way for voltage of terminals of antenna as a function of direction to the source also normalised to unity at maximum.

Recieving antenna's pattern is same as that of the transmitting antenna by

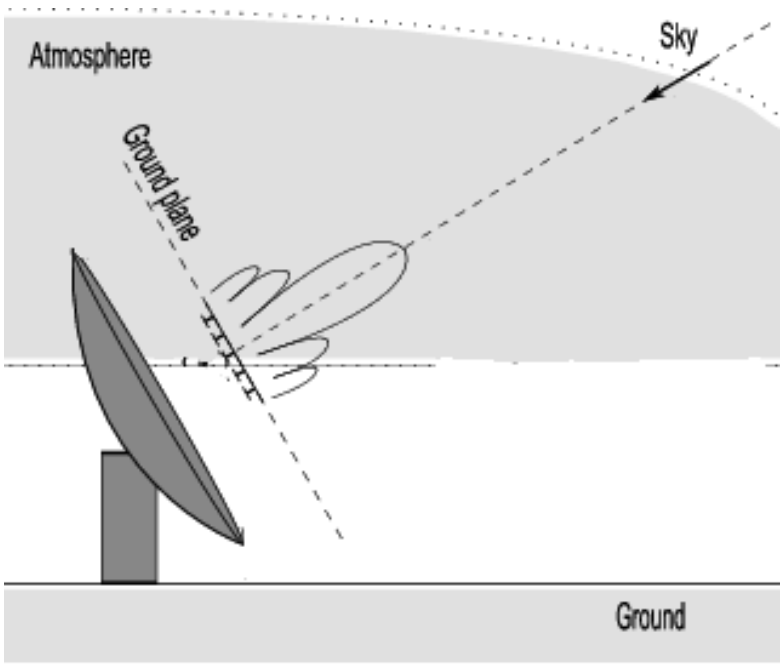

Figure 6.1: How an antenna actually 'sees' the source. [13]

the property of *reciprocity* that follows from the Maxwell's equations. It thus implies that, electric field far from a transmitting antenna, normalised to unity at maximum, is the field pattern.

We also know that power is proportional to the square of electric field, then the power pattern is the square of the field pattern, and is thus real and semi-definite.

Figure 6.2 shows a typical power pattern. The characteristic features to note are the mainlobe and the severeal subsidiary maxima called the sidelobes. The points at which the main lobe falls to half the maximum value are called the Half Power Points and the angular distance between these points is called the Half Power Beamwidth(HPBW). The minima of power pattern are called nulls.

In order to not confuse the nearby sources with one another, we would want to keep the HPBW small. Similarly to minimise the stray radiation, the sidelobes should be low. Diffraction theory gives

$$\Theta_{HPBW} \sim \frac{\lambda}{D} \tag{6.4}$$

where D is the physical dimension of the telescope and both the wavelength and dimension of telescope are measured in same units which keeps Θ in radians.

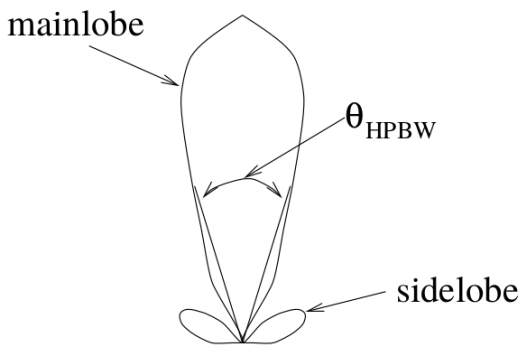

Figure 6.2: A Typical Power Pattern [4]

Directivity $D(\theta, \phi)$ and gain pattern $G(\theta, \phi)$ are defined as:

$$D(\theta, \phi) = \frac{\text{power emitted into}(\theta, \phi)}{\text{total power emitted}/4\pi} = \frac{4\pi P(\theta, \phi)}{\int P(\theta, \phi) d\Omega} \tag{6.5}$$

which being the transmitting pattern of the antenna, is the same as the receiving pattern within a constant factor, which we calculate below.

$$G(\theta, \phi) = \frac{\text{power emmitted into}(\theta, \phi)}{\text{total power input}/4\pi} \tag{6.6}$$

which is same as the directivity above, but with an efficiency factor. A figure of merit for reflector antennas is the aperture efficiency

$$\eta = \frac{A_e^{\max}}{A_g} \tag{6.7}$$

where A_g is the geometric cross sectional area of the main reflector. It can be atmost 1.0.

Assume a sky with brightness distribution $B(\theta)$ and a power pattern $A_e(\theta, \phi)$ as shown in the Figure 6.2 . Then the power actually available at the antenna terminals is the integral of the brightness in a given direction times the effective area in that particular direction, Figure 6.3

$$W(\theta') = \frac{1}{2} \int B(\theta) A_e(\theta - \theta') d\theta \tag{6.8}$$

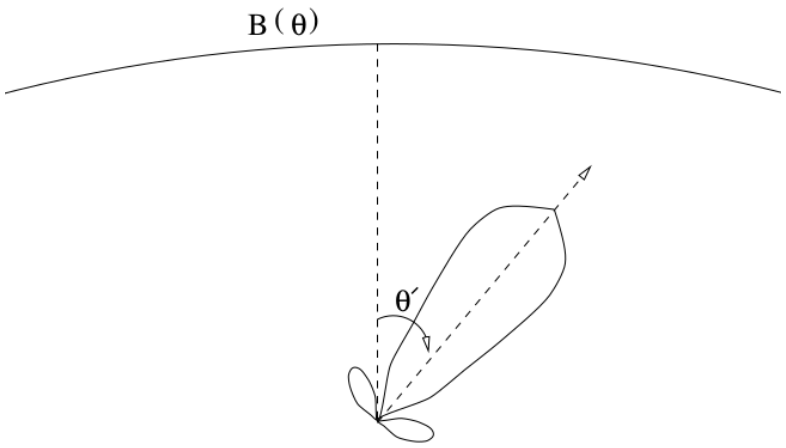

Figure 6.3: The antenna temperature is the convolution of sky brightness and the beam of the telescope. [4]

The available power is a function of θ' which gives the direction of telescope, the factor of half is for only one polarization absorbed. In two dimensions,

$$W(\theta', \phi') = \frac{1}{2} \int B(\theta, \phi) A_e(\theta - \theta', \phi - \phi') \sin\theta d\theta d\phi \tag{6.9}$$

which in temperature units is

$$T_A(\theta', \phi') = \frac{1}{2} \int \frac{T_B(\theta, \phi)}{\lambda^2} A_e(\theta - \theta', \phi - \phi') \sin\theta d\theta d\phi \tag{6.10}$$

$$T_A(\theta', \phi') = \frac{A_e^{max}}{\lambda^2} \int T_B(\theta, \phi) P(\theta - \theta', \phi - \phi') \sin\theta d\theta d\phi \tag{6.11}$$

Thus the antenna temperature is the weighted average of sky temperature, weighed by the power pattern of the antenna.

Only if the power pattern is a single infinitely sharp spike is the antenna temperature the same as the sky temperature. For all real telescopes, however, the antenna temperature is a smoothed version of the sky temperature. Supposing that you are making a sky survey for sources. Then a large increase in the antenna temperature could mean either that there is a source in the main beam,

or that a collection of faint sources have combined to give a large total power. From the statistics of the distribution of sources in the sky (presuming you know it) and the power pattern, one could compute the probability of the latter event. This gives a lower limit to the weakest detectable source, below this limit,(called the confusion limit), one can no longer be confident that increases in the antenna temperature correspond to a single source in the main beam. The confusion limit is an important parameter of any given telescope, it is a function of the frequency and the assumed distribution of sources.

If we consider an antenna terminated in a resistor, with the entire system being placed in a black box at temperature T, then after thermal equilibrium has been reached, the power flowing from the resistor to the antenna is

$$P_{R\to A} = kT \tag{6.12}$$

The power flow from the antenna to the resistor from equation 6.11 and assuming the sky temperature is same everywhere

$$P_{A\to R} = \left(\frac{A_e^{max} kT}{\lambda^2}\right) \int P(\theta,\phi) d\Omega \tag{6.13}$$

Since in thermal equilibrium, the net power flow goes to zero, we obtain the following relationship

$$A_e max = \frac{\lambda^2}{\int P(\theta, \phi d\Omega)} \tag{6.14}$$

which implies that only the shape of power pattern determines the maximum effective aperture. For example, a narrow pattern would imply a higher aperture efficiency. For a reflecting telescope,

$$\int P(\theta,\phi) d\Omega \sim \Theta^2_{HPBW} \sim \left(\frac{\lambda}{D}\right)^2 \tag{6.15}$$

$$A_e^{max} \sim D^2 \tag{6.16}$$

From 6.14,

$$A_e = A_e^{max} P(\theta, \phi) = \frac{\lambda^2 P(\theta, \phi)}{\int P(\theta, \phi) d\Omega} \tag{6.17}$$

Finally, on comparison with equation 6.5 we see the constant factor that relates the effective area with directivity as

$$D(\theta, \phi) = \frac{4\pi}{\lambda^2} A_e(\theta, \phi) \tag{6.18}$$

6.2 Computing An Antenna Pattern

Take the case of a parabolic reflecting telescope with feed at the focus. The radiation from the feed reflects off the telescope and is beamed off into space. If we knew the radiation pattern of the feed, then by using geometric optics we could calculate the electric field on the aperture plane. Also, if the telescope was infinitely large, then the electric field would have been a plane wave in the aperture plane. Since a plane wave would propagate as it is through free space, the far field would simply be a plane wave travelling along the axis of the reflector. The power pattern would be an infinitely narrow spike diminishing everywhere else.

In reality, telescopes are finite in size, which means that diffraction comes into the picture. Consider a one dimensional aperture, of length l, with electric field distribution or aperture illumination $e(x)$. Then the field at point $P(r, \theta)$ due to a point source at a distance of x from the center of the aperture, according to the Huygen's principle is

$$dE = \frac{e(x)}{r^2} e^{\frac{2\pi x \sin\theta}{\lambda}} \tag{6.19}$$

here $r >> l$, x $\sin\theta$ is simply the difference in path length between the path from

the center of the aperture to the point P and the path from x to point P. Since the wave from point x has a shorter path length, it arrives at point P at an earlier phase. The total electric field at P is:

$$E(r,\theta) = \int_{-l/2}^{l/2} \frac{e(x)}{r^2} e^{-jk\mu x} dx \tag{6.20}$$

where $k = 2\pi/\lambda$ and $\mu = \sin\theta$ and x is now measured in wavelengths. The shape of the distribution is clearly independent of r, and hence the unnormalized power pattern is

$$F_U(\mu) = \int_{-\infty}^{\infty} e_1(x) e^{-jk\mu x} dx \tag{6.21}$$

where

$$e_1(x) = e(x) \quad \text{if} \quad |x| \geq l/2; \quad 0 \quad \text{otherwise} \tag{6.22}$$

For a 1D uniformally illuminated aperture of length l. The far field then is

$$E(\mu) = \int_{-l/2}^{l/2} e^{\frac{-j2\pi x\mu}{\lambda}} dx \tag{6.23}$$

$$= \lambda \frac{\sin(\pi l/\lambda\mu)}{\pi\mu} \tag{6.24}$$

and the normalized field pattern is

$$F(\mu) = \frac{\sin(\pi l/\lambda\mu)}{\pi l/\lambda\mu} \tag{6.25}$$

This is the 1D sinc function, with the first null at $\mu = \lambda/l$, the first sidelobe at $\mu = 3/2(\lambda/l)$ with strength $2/3\pi$. This means that the strength of the power pattern is $(2/3\pi)^2 = 4.5\%$, which shows that

- The width of a function is inversely proportional to the width of its transform. This means that large antennas will have smaller beams.

- Sharp discontinuities in the function will give rise to sidelobes - called ringing - in the Fourier transform.

Aperture illumination design hence involves the following tradeofs

- A tapered illumination has a broader main beam or equivalently a smaller aperture but also lower sidelobes than uniform illumination.
- If the illumination is high towards the edges then unless there is a very rapid cutoff, which causes higher sidelobes, there will be a lot of spillover.

Chapter 7

Mapping the Sky

We now look at the coordinate systems used in practical aperture synthesis in detail.

7.1 Angular coordinates

The response of an interferometer

$$r(\tau(t)) = \cos(2\pi\nu_o\tau) \tag{7.1}$$

where we take incoming radiation to be quasi-monochromatic, the source as a point source located at the phase center, and $\tau = \tau_o = (D/c)\sin(\theta(t))$ as the geometric delay with θ being the direction which the antennas are tracking w.r.t the vertical direction, λ the wavelength, ν_o the center frequency of the observing band and D the separation between the antennas.

As the Earth rotates and the antennas track this source, the delay changes with time which is exactly compensated by a computer controlled delay. For a point source at the phase center, the output of the interferometer is the amplitude of the fringe pattern.

For a source at $\theta = \theta_o + \Delta\theta$, for small $\Delta\theta$, $\tau = \tau_o + \Delta\theta(D/c)\cos\theta(t)$ Now fringe stopping compensates for τ_o, then response of the interferometer for this source is

$$r(\tau(t)) = \cos(2\pi\Delta\theta D_\lambda \cos\theta) \tag{7.2}$$

where $D_\lambda = D/\lambda$. If the phase center itself is shifted by an equivalent of $\lambda/4$, the response picks up a phase of $\pi/2$ and becomes sinusoidal instead of co-sinusoidal. This shows that the interferometer will now respond to both odd and even parts of the brightness distribution and we write it in a complex notation as:

$$r(\tau(t)) = e^{2\pi i \Delta\theta D_\lambda \cos\theta} \tag{7.3}$$

As $D_\lambda \cos\theta$ is the projected separation between the antennas in units of wavelength int the direction normal to the phase center, we substitute it as u, also see that $l = \sin(\Delta\theta)\ \Delta\theta$, the response then is given as

$$r(u, l) = e^{2\pi i u l} = e^{2\pi i u \Delta\theta} \tag{7.4}$$

If the normalized power reception pattern of antennas, all assumed to be identical, at a given frequency is $B(\Delta\theta)$ and the surface brightness be $I(\Delta\theta)$, then the response of our interferometer for a point source located $\Delta\theta$ away from the phase center will be

$$r(u, \Delta\theta) = I(\Delta\theta)B(\Delta)\theta e^{2\pi i u \Delta\theta} \tag{7.5}$$

and for an extended source with a continuous surface brightness distribution,

$$V(u) = \int B(\Delta\theta)I(\Delta\theta)e^{2\pi i u \Delta\theta} d\Delta\theta = \int B(l)I(l)e^{2\pi i u l} dl \tag{7.6}$$

This is a one dimensional Fourier Transform relationship between the source brightness distribution and the visibility function. Although the integral is over the entire sky visible to antennas, it is finite only for a range of l given by the antenna primary reception pattern $B(l)$. Thus, l specifies the direction of source flux relative to the pointing center, u then has the interpretation of spatial frequency and $V(u)$ represents the 1D spatial frequency spectrum of this source.

7.2 Astronomical Coordinate System

We mostly employ azimuth and elevation angles with respect to different origins and orientation of axes in order to specify source positions. Most commonly used is the Equatorial Coordinate system where Right Ascension(RA) and Declination(δ) are defined. RA is the azimuthal angle from the first point of Aries [1], while δ is the elevation of the source from the normal to the celestial equator. Since there are two possible directions for RA, it is measured from the equinox towards the east.

The position of the source in the sky in this coordinate system remains constant as the Earth rotates, and the azimuth/elevation of antennas that rotate with Earth are constantly adjusted to track the point in the sky.

The changing position of the sources in the sky as seen by the observer on the surface of the Earth is specified by replacing RA by the Hour Angle (HA) which is the azimuth of the source measured in units of time, with respect to the local meridian of the source with $HA = -6^h$ pointing due East.

7.3 Physical Coordinate System

The antennas are located on the surface of the Earth, and therefore rotate with respect to the source in the sky. For employing techniques in aperture synthesis, the antenna positions are specified in a coordinate system so that the separation of antennas is the projected separation in plane normal to the phase center. In other words, in this system, the separation between the antennas is as seen by the observer sitting in the phase center reference frame.

The figure 7.1 depicts a right handed (u, v, w) coordinate system. The u axis is along the astronomical E-W direction and v axis along the N-S direction. The (u, v) plane is parallel to the tangent plane in the direction of phase center on the celestial sphere while w points in the direction of interest, usually kept as the phase center.

[1]The celestial equator meets the ecliptic plane at two points, one is the first point of Aries and the other first point of Libra. The former is chosen as the 'prime meridian' for calculating RA for historical reasons.

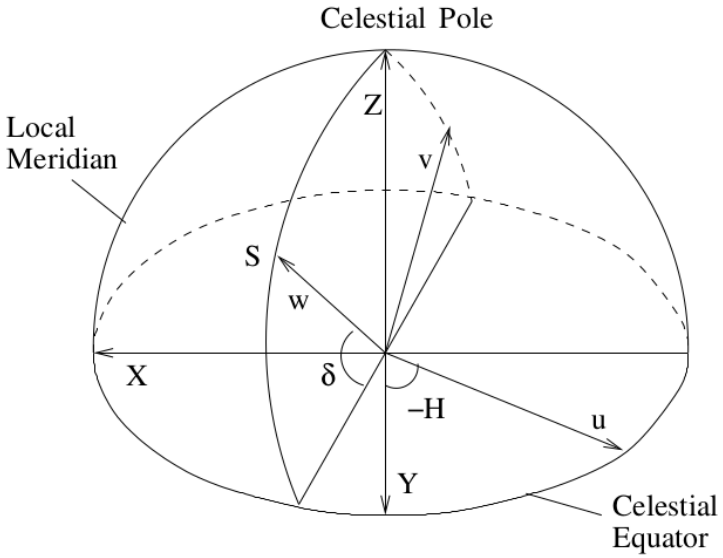

Figure 7.1: Relationship between different coordinate systems. [4]

As the Earth rotates, the (u, v) plane rotates with the source in the sky, changing the (u, v, w) coordinates of the antennas generating tracks in the uv-plane.

Now the u coordinate of one antenna is with respect to the other antenna making the interferometer which is located at the origin. If this origin is arbitrarily located and the coordinates are u_1 and u_2, then equation 7.5 becomes

$$r(u, l) = e^{2\pi i(u_1 - u_2)l} \tag{7.7}$$

We can see that only the difference matters, so we can work with *baseline vectors* specified as the difference between the position vectors of various antennas in the (u,v,w) coordinates.

7.4 Coordinate Transformation

As we have seen, the (u,v,w) coordinates of antennas lie in the 'imaging' coordinate system while antennas are actually located in the terrestrial coordinate system.

This terrestrial coordinate system is a right handed Cartesian coordinate system. The (X,Y) plane is parallel to the Earth's equator, X is in the meridian plane and Y towards East, and Z points towards the celestial pole. In terms of astronomical coordinate system (HA, δ), the axes will be defined as $X = (0^h, 0^o), Y =$

$(-6^h, 0^o), Z = (\delta = 90^o)$. If the components of D_λ are $(X_\lambda, Y_\lambda, Z_\lambda)$ then the components in the (u, v, w) coordinate system can be determined by the following transformation

$$\begin{bmatrix} u \\ v \\ w \end{bmatrix} = \begin{bmatrix} \sin(HA) & \cos(HA) & 0 \\ -\sin(\delta)\cos(HA) & \sin(\delta)\sin(HA) & \cos(\delta) \\ \cos(\delta)\cos(HA) & -\cos(\delta)\sin(HA) & \sin(\delta) \end{bmatrix} \begin{bmatrix} X \\ Y \\ Z \end{bmatrix}$$

As the Earth rotates, the hour angle changes giving different set of (u, v, w) coordinates for each antenna pair at each instant of time. The locus of projected antenna spacings u and v defines an ellipse with hour angle as the variable

$$u^2 + \left(\frac{v - Z\cos\delta_o}{\sin\delta_o} \right)^2 = X^2 + Y^2 \tag{7.8}$$

where (HA_o, δ_o) define the phase center direction. This ellipse is referred to as the uv-track and the pattern generated by the uv points sampled by the entire array of antennas over the period of observation is referred to as the uv coverage.

The uv points close to the origin form the shorter baselines, provide low resolution information and are sensitive to the coarse structure of the source. The uv points away from the origin create the longer baselines provide higher resolution and thus sensitive to finer details. Just by looking at the uv coverage plots we can observe that, smaller baselines are more sensitive than the longer baselines just by virtue of the fact that for a given observation time period, there are more points of observation near the center while lesser number outside. Obviously, sensitivity is zero where there are no points.

The uv coverage depends on the position of the source in the astronomical coordinate system. The reference in the astronomical coordinate system is the line of intersection of the ecliptic and the equatorial planes. Since this reference line changes due to precession of Earth's rotation axis, the uv coverage in turn becomes a function of the reference epoch for which the source is specified. Thus, for consistency, all source positions are specified in standard epochs (B1950 or J2000). Since each point in the (u, v, w) plane measures a particular spatial frequency and this spatial frequency coverage differs from one epoch to another, it is necessary

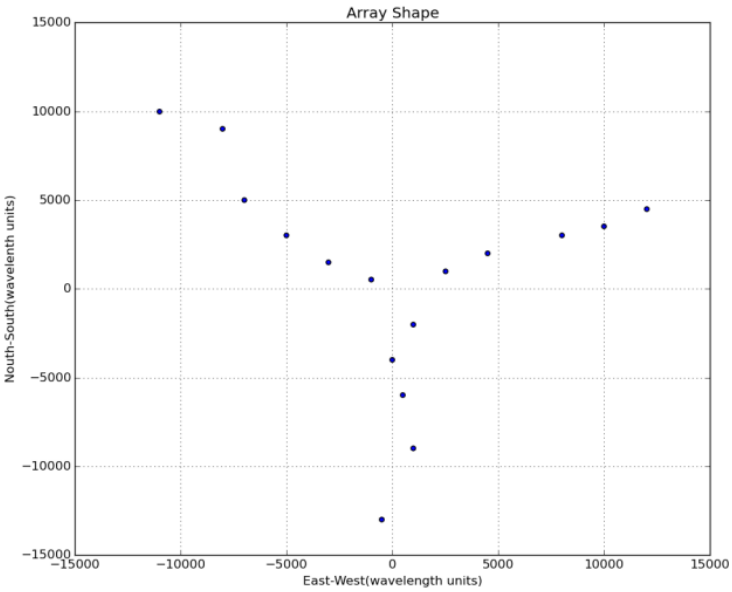

Figure 7.2: The array shape of the GMRT

to precess the source coordinates to the current epoch prior to observations; all processing of the visibility data for the purpose of mapping must be done with (u, v, w) evaluated for the epoch of observations. But precessing the visibilities to the standard epoch before inverting will require specifying the real and imaginary parts of the visibility at coordinates which are in fact not measured - since the coverage changes with epoch - this introduces errors in the mapping procedures. However, this change is very slow, happening over years and decades.

7.5 Generalised 2D Fourier transform relation

In the following discussion we assume monochromatic radiation with negligible frequency bandwidth and that the (u, v) measurements are instantaneous measurements.

Let the vector $\bar{L}_o$ give the direction of the phase center,and $\bar{D}_\lambda$ represent the location of all the antennas of an array with respect to a reference antenna. Then,

$$\tau_g = \bar{D}_\lambda . \bar{L}_o \tag{7.9}$$

Also, note that $2\pi \bar{D}_\lambda . \bar{L}_o = 2\pi w$ is the phase by which visibility should be rotated to stop the fringe. For any source direction, $\bar{L} = \bar{L}_o + \bar{\sigma}$, the output of the inter-

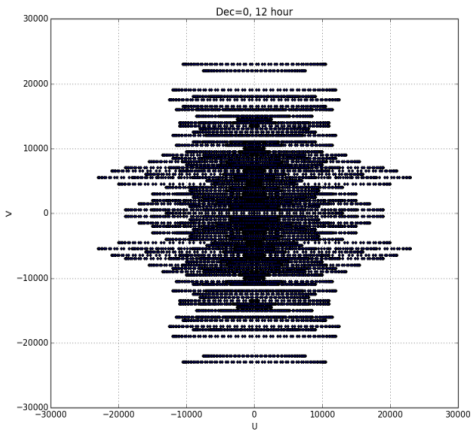

(a) 12 hr synthesis image for dec = 0^o

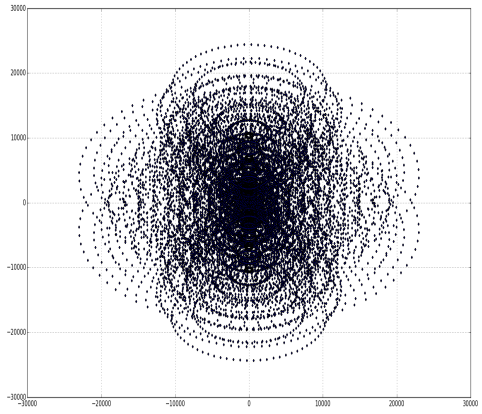

(b) 12 hr synthesis image for dec = 40^o

Figure 7.3: u versus v plot for two different declination angles for the GMRT array.

ferometer after fringe stopping will be

$$V(\bar{D}_\lambda) = \int_{4\pi} I(\bar{L})B(\bar{L})e^{2\pi i \bar{D}_\lambda.(\bar{L}-\bar{L}_o)}d\Omega \tag{7.10}$$

If $\bar{L}$ is (l, m, n) in the sky tangent plane, $\bar{L}_o$ is unit vector along the w axis, and $\bar{D}_\lambda$ is (u, v, w), then

$$\bar{D}_\lambda.\bar{L} = ul + vm + wn \tag{7.11}$$

and

$$\bar{D}_\lambda.\bar{L}_o = w \tag{7.12}$$

and

$$d\Omega = \frac{dldm}{n} = \frac{dldm}{\sqrt{1 - l^2 - m^2}} \tag{7.13}$$

giving

$$V(u, v, w) = \int\int I(l, m)B(l, m)e^{2\pi i(lu+mv+w(\sqrt{1-l^2-m^2}-1))}\frac{dldm}{\sqrt{1 - l^2 - m^2}} \tag{7.14}$$

Note that the complex visibility is a function of the coordinates (u, v, w) since these represent the spacing of the antennas with respect to the phase tracking center of the source.

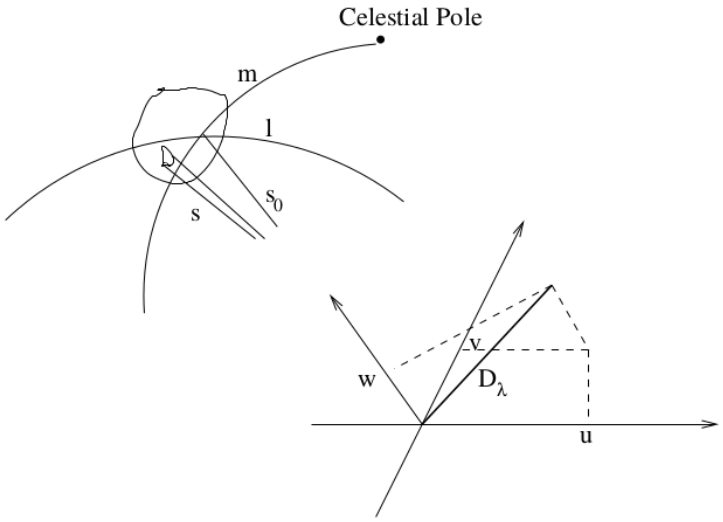

Figure 7.4: Relationship between (l, m) and (u, v, w) coordinates [4]

In the situation of the array being exactly in plane, w being exactly zero, this relation would reduce to an exact 2D Fourier Transform relation. This is true for East-West arrays like the WSRT, the ATCA.

In order to maximise uv coverage, the arrays should not be exactly East-West, like the GMRT or VLA. Now, if the field of view being mapped is small, ie for small l and m, $\sqrt{1-l^2-m^2}$ can be neglected which gives

$$V(u,v,0) = \int\int I(l,m)B'(l,m)e^{2\pi i(ul+vm)}dldm \tag{7.15}$$

where $B' = B/\sqrt{1-l^2-m^2}$, and this is a Fourier transform relation.

As there are a finite number of antennas, the uv coverage is not continuous. We define a *sampling function* as:

$$S(u_k, v_k) = \delta(u-u_k, v-v_k) \tag{7.16}$$

which means the value of S is one for all sampled (u,v) points and zero everywhere else. Then in reality, equation 7.15 becomes

$$V(u,v)S(u,v) = \int\int I(l,m)e^{2\pi i(lu+mv)}dldm \tag{7.17}$$

Since the visibility function for a point source at the (l, m) origin is a constant in u and v, the Fourier transform of the transfer function indicates the response to a point source i.e. the synthesized beam. Inverting the above equation, and using the convolution theorem, we get

$$I^D = I * DB \tag{7.18}$$

Here, DB i.e the *Dirty Beam* is the Fourier Transform of S. I^D is the raw image produced by an Earth rotation aperture synthesis telescope, is called the *Dirty Map*.

The assumptions of monochromaticity and instantaneous measurements is not true in real life. Observations for continuum mapping are made with as large a frequency bandwidth as possible so as to maximize sensitivity and the data are recorded after finite integration. Both the issues result in the degradation in the map plane.

The approximation of w term being zero implies that the source brightness distribution is limited to the tangent plane at the phase center in the sky rather than on the surface of the celestial sphere. However, at low frequencies where antenna primary beams are larger and radio emission is also on a larger scale, this assumption restricts the mappable part of the sky to a fraction of the primary beam!

Chapter 8

The van Cittert Zernike Theorem

It relates the spatial coherence function $V(\mathbf{r}_1, \mathbf{r}_2) = \langle E(r_1)E^*(r_2)\rangle$ to the distribution of intensity of incoming radiation $\mathcal{I}(s)$. We can show that the spatial correlation function depends only on the difference $\mathbf{r}_1 - \mathbf{r}_2$, and if the measurements are in plane, then

$$V(r_1, r_2) = \mathcal{F} \tag{8.1}$$

where $\mathcal{F}$ implies taking the fourier transform. We now derive this relation [4].

Assuming that the source is distant and that it can be approximated as a brightness distribution on the celestial sphere of radius R as shown in figure 8.1. Let the electric field at a point $P_1'(x_1', y_1', z_1')$ at the source be given by $\mathcal{E}(P_1')$ then the field $E(P_1)$ at the observation point $P_1(x_1, y_1, z_1)$ is given as

$$E(P_1) = \int \mathcal{E}(P_1')\frac{e^{-ikD(P_1', P_1)}}{D(P_1', P_1)}d\Omega_1 \tag{8.2}$$

where $D(P_1', P_1)$ is the distance between P_1' and P_1. Here we have assumed that the electric field is a scalar. Now if $E(P_2)$ is the field at some other observing point $P_2(x_2, y_2, z_2)$ then the cross correlation between these two fields is given as

$$\langle E(P_1)E^*(P_2)\rangle = \int \langle \mathcal{E}(P_1')\mathcal{E}(P_2')\rangle \frac{e^{-ik(D(P_1', P_1) - D(P_2', P_2))}}{D(P_1', P_1)D(P_2', P_2)}d\Omega_1 d\Omega_2 \tag{8.3}$$

Further assumption that the radiation from astronomical objects is not spatially

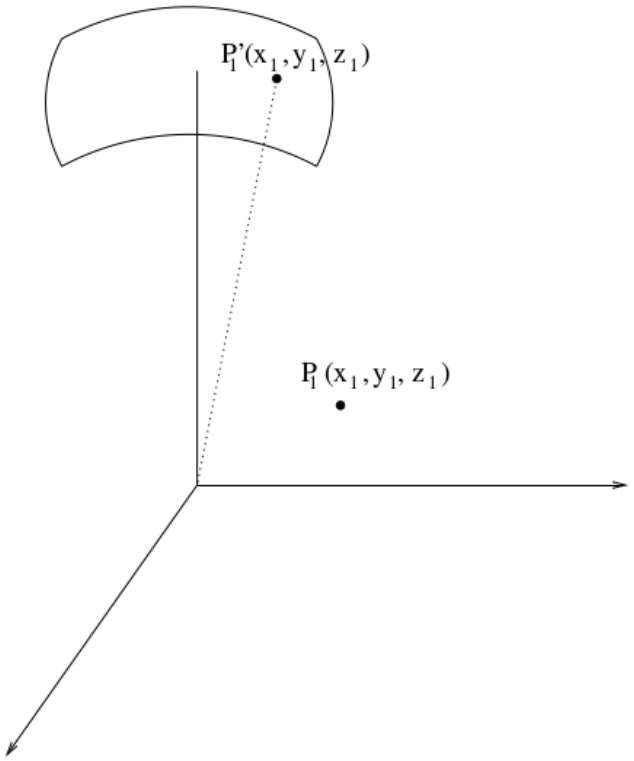

Figure 8.1: Geometry for van Cittert Zernike theorem. [4]

coherent, i.e. $\langle \mathcal{E}(P_1')\mathcal{E}^*(P_2')\rangle = 0$ except for $P_1' = P_2'$, then

$$\langle E(P_1)E^*(P_2)\rangle = \int \mathcal{I}(P_1')\frac{e^{-ik(D(P_1',P_1)-D(P_2',P_2))}}{D(P_1',P_1)D(P_2',P_2)}d\Omega_1 \tag{8.4}$$

where $\mathcal{I}(P_1')$ is the intensity at point P_1'. Our assumption that the source lies on the celestial sphere of radius R gives $x_1' = R\cos(\theta_x) = Rl$, $y_1' = R\cos(\theta_y) = Rm$, $z_1' = R\cos(\theta_z) = Rn$ where (l, m, n) are direction cosines. It is clear that $l^2 + m^2 + n^2 = 1$ and $d\Omega = \frac{dldm}{\sqrt{1-l^2-m^2}}$

$$\begin{aligned}
D(P_1', P_1) &= [(x_1' - x_1)^2 + (y_1' - y_1)^2 + (z_1' - z_1)^2]^{1/2} && (8.5)\\
&= [(Rl - x_1)^2 + (Rm - y_1)^2 + (Rn - z_1)^2]^{1/2} && (8.6)\\
&= R[(l - x_1/R)^2 + (m - y_1/R)^2 + (n - z_1/R)^2]^{1/2} && (8.7)\\
&\approx R[(l^2 + m^2 + n^2) - 2/R(lx_1 + my_1 + nz_1)]^{1/2} && (8.8)\\
&\approx R - (lx_1 + my_1 + nz_1) && (8.9)\\
& && (8.10)
\end{aligned}$$

Substituting this back,

$$\langle E(P_1)E^*(P_2)\rangle = \frac{1}{R^2}\int \mathcal{I}(l,m)\frac{e^{-ik[l(x_2-x_1)+m(y_2-y_1)+n(z_2-z_1)]}}{\sqrt{1-l^2-m^2}}dldm \tag{8.11}$$

Intensity is a function of only (l, m) since they are sufficient to uniquely define a point on the sphere as $l^2 + m^2 + n^2 = 1$. The spatial correlation function $\langle E(P_1)E^*(P_2)\rangle$ is also referred to as the visibility $\mathcal{V}(u, v, w)$.

In terms of baseline coordinates, $u = (x_2 - x_1)/\lambda, v = (y_2 - y_1)/\lambda, w = (z_2 - z_1)/\lambda$ and ignoring the constant factor

$$\mathcal{V}(u,v,w) = \int \mathcal{I}(l,m)e^{-i2\pi[lu+mv+nw]}\frac{dldm}{\sqrt{1-l^2-m^2}} \tag{8.12}$$

This relation between the source brightness and the visibility is referred to as the van Cittert Zernike Theorem.

Chapter 9

Wide field observations

9.1 Cartesian Basis

Recall that the original expression for visibility was

$$V(u,v,w) = \int\int I(l,m)B(l,m)e^{-2\pi i[lu+mv+\sqrt{1-l^2-m^2}w]}\frac{dldm}{\sqrt{1-l^2-m^2}} \tag{9.1}$$

Only in the small FoV limit ($l^2 + m^2 << 1$) or in the case where antennas were arranged in E-W line, did this relation become a simple 2D Fourier Transform. In more practical situations, antennas are arranged in arrays that maximize uv coverage, for example the Y shaped GMRT array. The FoV of a telescope is limited by the primary beams of the antennas. If the observations are to be made at larger FoV, the full expression above needs to be used to map full primary beams of the antennas. Thus wide field imaging requires non-trivial handling of the third term - $w\sqrt{1-l^2-m^2}$ called the w term.

Interpreting the w-term A wavefront originating from the phase center direction is received by all the antennas and the signal is multiplied in-phase at the correlator, effectively phasing the array. As is obvious, the celestial sphere is the locus of all the points in the 3D space for which the array will remain phased. Therefore, away from the phase center, the wavefront will carry an extra phase which is due to its separation from the center and not the geometry of the array. Thus, this term carries information about the source's structure.

Then the 2D approximation for a small FoV takes the form of approximating the sky by a 2D plane close to the phase center and ignoring this w term. But, for a source far away, we need to rotate visibility by this w term so as to continue the 2D approximation for that source, which is equivalent to shifting the phase center and thus shifting the equivalent point in the image plane. This shift is, as expected, different for each part of the image since the w term depends on the image coordinates, and thus a constant phase rotation of all the visibilities would not of be of much effect in removing errors due to removal of the w term.

9.2 Spherical Basis

As we have understood, many issues arise due to the 3D nature of the problem at hand. Deconvolution to obtain the Brightness function, followed by handling the w term in the wide FoV regime are difficulties that have the power to, even in principle, accommodate a lot of errors. We now look at another method of doing the same things, only simpler.

Carozzi in 2015 [1] proposed the use of spherical basis, instead of the usual Cartesian, for the geometry here seems to follow the same. The relation derived here is inherently wide field.

For the sake of illustration, we assume that the electric field is scalar and not polarized. The relation can be easily generalized to other components.

Begin with the scalar intensity component of the extended vCZ theorem[2] i.e. relation between visibility V and the brightness B on the celestial sphere as

$$V_I(\mathbf{r}, k) = \int B_I(\Omega_k) e^{-i\mathbf{k}.\mathbf{r}} d\Omega_k \tag{9.2}$$

where $\mathbf{r}$ is the baseline vector, $\mathbf{k}$ is the wavevector, $\Omega_k = (\theta_k, \phi_k)$ are the angular components of $\mathbf{k}$ on the celestial sphere.

The subscript k denote that the angles refer to the spherical components of the wavevector. Now, if measurements are considered in vacuum, then the wavenumber $k = |\mathbf{k}|$ is given by the frequency (used for measurements of visibility) divided

by the speed of light, $k = \frac{2\pi\nu}{c}$.

The subscript I denotes the Stokes I component - the scalar flux density. If we only deal with this component, we can discard this subscript for further calculations. The phase reference position is taken to be as origin.

Observe that the equation 9.2 satisfies the Helmholtz wave equation. Operate with Laplace on both sides and obtain,

$$\nabla^2 V + k^2 V = 0 \tag{9.3}$$

This is the wave equation in the visibility domain. Recall that it has solutions in both Cartesian and Spherical coordinates.
Therefore eigenfunctions of the spherical wave equation, given as

$$j_l Y_{lm}(\theta, \phi) \qquad for\ l = 0, 1, 2...\ and\ m = -l, ..., l$$

should produce a vCZ relation. The boundary condition put in here says that the visibility should be finite at the origin. The $Y_{lm}(\Omega)$ is the usual orthonormal spherical harmonic function where l and m are the polar and azimuthal quantum numbers respectively. The $j_l(kr)$ is the spherical Bessel function of the first kind.

Using the plane wave decomposition formula

$$e^{(-i\mathbf{k}.\mathbf{r})} = 4\pi \sum_{l=0}^{\infty} \sum_{m=-l}^{l} (-i)^l j_l(kr) Y_{lm}(\theta_r, \phi_r) Y *_{lm} (\theta_k, \phi_k) \tag{9.4}$$

Substituting this in equation 9.2 as,

$$V = \int B(\Omega_k) \left(4\pi \sum_{l=0}^{\infty} \sum_{m=-l}^{l} (-i)^l j_l(kr) Y_{lm}(\theta_r, \phi_r) Y^*_{lm}(\Omega_k) \right) d\Omega_k \tag{9.5}$$

$$= 4\pi \sum_{l=0}^{\infty} \sum_{m=-l}^{l} (-i)^l j_l(kr) Y_{lm}(\theta_r, \phi_r) \int B(\Omega_k) Y^*_{lm}(\Omega_k) d\Omega_k \tag{9.6}$$

Expanding the brightness function in the basis of spherical harmonics,

$$B(\Omega_k) = \sum_{l=0}^{\infty} \sum_{m=-l}^{l} b_{lm} Y_{lm}(\Omega_k) \tag{9.7}$$

where b_{lm} will be the multipole moments of the sky. Substitute this back in equation 9.6 and obtain,

$$V = 4\pi \sum_{l=0}^{\infty} \sum_{m=-l}^{l} (-i)^l j_l(kr) Y_{lm}(\theta_r, \phi_r) \int \left(\sum_{l=0}^{\infty} \sum_{m=-l}^{l} b_{lm} Y_{lm}(\Omega_k) \right) Y^*_{lm}(\Omega_k) d\Omega_k \tag{9.8}$$

Using the orthogonality relation of the spherical harmonics,

$$\int_0^{4\pi} Y_{lm}(\Omega) Y^*_{l'm'}(\Omega) d\Omega = \delta_{ll'} \delta_{mm'} \tag{9.9}$$

we obtain

$$\mathcal{V} = 4\pi \sum_{l=0}^{\infty} \sum_{m=-l}^{l} (-i)^l j_l(kr) Y_{lm}(\theta_r, \phi_r) b_{lm} \tag{9.10}$$

Also expanding the visibility distribution in terms of the eigenfunctions of the wave equation

$$\mathcal{V} = \sum_{l=0}^{\infty} \sum_{m=-l}^{l} \tilde{v}_{lm} j_l(kr) Y_{lm}(\Omega_r) \tag{9.11}$$

Inserting this in equation 9.10, we get

$$\sum_{l=0}^{\infty} \sum_{m=-l}^{l} \tilde{v}_{lm} j_l(kr) Y_{lm}(\Omega_r) = 4\pi \sum_{l=0}^{\infty} \sum_{m=-l}^{l} (-i)^l b_{lm} j_l(kr) Y_{lm}(\theta_r, \phi_r) \tag{9.12}$$

Again, applying orthonormality of the spherical harmonics, we obtain a simple proportionality relation as

$$\tilde{v}_{lm} = 4\pi (-i)^l b_{lm} \tag{9.13}$$

We can take this calculation further, and see that the above Brightness function is a convolution of the Intensity function and the Antenna Pattern as

$$B(\Omega_k) = \int I(\Omega) A(\Omega - \Omega_k) d\Omega \tag{9.14}$$

We now expand the functions $B(\Omega_k)$ and $I(\Omega)$ as

$$B(\Omega_k) = \sum_l \sum_m b_{lm} Y_{lm}(\Omega_k) \tag{9.15}$$

$$I(\Omega) = \sum_l \sum_m i_{lm} Y_{lm}(\Omega) \tag{9.16}$$

which upon substituting in equation 9.14 yields

$$\sum_l \sum_m b_{lm} Y_{lm}(\Omega_k) = \int \sum_l \sum_m i_{lm} Y_{lm}(\Omega) A(\Omega - \Omega_k) d\Omega \tag{9.17}$$

and, for a given l and m value set,

$$b_{lm} = i_{lm} Y^*_{lm}(\Omega_k) \int Y_{lm}(\Omega) A(\Omega - \Omega_k) d\Omega \tag{9.18}$$

We almost always are aware of the antenna patterns for our telescopes as a function of the angular coordinates. Thus, this relation determines the Intensity components i_{lm}.

Comparing equations 9.13 and 9.18, we can see that we have finally obtained a direct relationship between the required Intensity function and the measured Visibility. This expression is a much simpler version of the Cartesian counterpart, and is easily computed.

Chapter 10

Case Study I: Ooty Wide Field Array

10.1 Design

Located at Ootacamund in southern part of India, the Ooty Wide Field Array (OWFA) is of the cylindrical paraboloid variety. This 530 m long (North-South) and 30 m wide (East-West) telescope operates at a center frequency of 326.5 MHz, i.e. about one meter long wavelength, with a 15 MHz bandwidth.

It is strategically placed on a hill that has a slope of about 11^o equal to the latitude of the place which implies that it is naturally an equatorial mount.

The reflecting surface is a set of 1100 stainless steel wires, each 530 m long, 0.38 mm in diameter and supported by 24 parabolic frames separated by 23 m from each other.

The reflector is an offset type reflector, in that, the feed eventhough located at the focal point of the reflector, does not obstruct the FoV. This is because the reflector is an asymmetric segment of the parabola and therefore keeps the focus offset to one side of the reflector.

1056 dipoles arranged in a linear and uniform array along the focal line illuminate the focal reflector.

Mechanical rotation through a common driveshaft of the telescope steers it along the East-West, while the North-South steering is obtained by introducing delays.

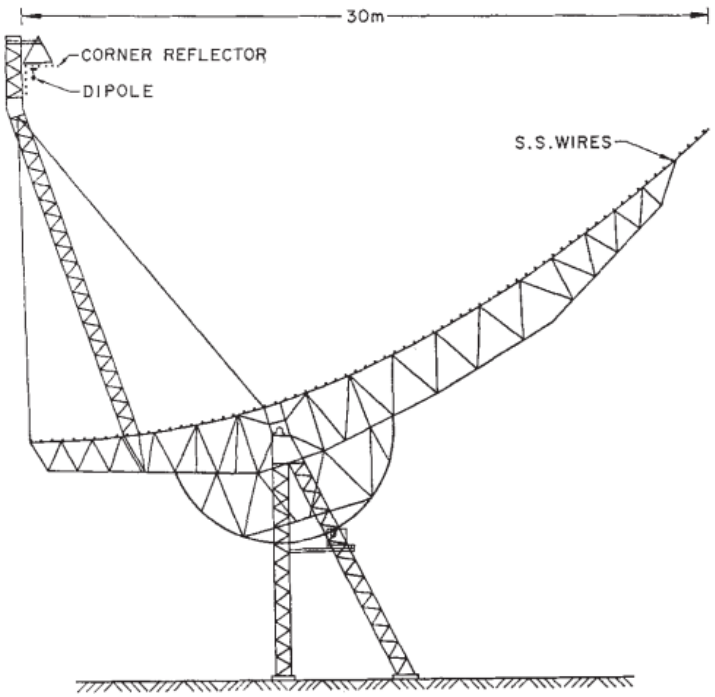

Figure 10.1: The geometry of the OWFA antenna. [14]

One antenna element is a combination of 4 dipoles, making a total of 264 antenna elements for 1056 dipoles. Each such antenna element is 1.9m long along the length of the cylinder and 30m wide. The smallest baseline thus corresponds to 1.9m and the longest to 505m.

10.2 Wide field observations with OWFA

The primary beam pattern decides the FoV of the interferometer. For OWFA, this FoV is asymmetric with FWHM of 1.75^o corresponding to 30m width in the East-West direction, and a FWHM of 27.4^o in North South direction.

We consider a case where we have one antenna observing one source in the sky. The antenna remains fixed while the source moves. We take the phase center at the center of the FoV, mark it as the origin, and point the antenna towards this direction. We consider the same dipole like antenna as the OWFA, and make it a simple one dimensional problem. This means that we take only one baseline into consideration, $B = 1.9m \sim 2m$ and consider zero change in the azimuthal coordinate of the source.

The antenna pattern along this baseline for OWFA is a Gaussian function. Another added simplicity is that we take the Intensity function I as a Delta function. The source moves from $\theta = 0$ radian to $\theta = 1$ radian. This is far beyond the FoV of the antenna, and thus we are in the wide field regime.

According to the Cartesian method,

$$V(u,v,w) = \int I(l,m)A(l,m)e^{-i2\pi[lu+mv]}\frac{dldm}{\sqrt{1-l^2-m^2}} \tag{10.1}$$

we can see that a wide field regime implies taking care of the damping term in the denominator i.e. $\sqrt{1-l^2-m^2}$.

We plot the visibility measurements of this source using the Fourier method for two antenna patterns - Gaussian and Sinc functions, for different values of the baseline. The antenna patterns were taken to be

$$A_{sinc} = sinc^2\left(\frac{\pi l_o B}{\lambda}\right) \tag{10.2}$$

and

$$A_{gauss} = exp\left(-\frac{1}{2}\frac{\pi l_o B}{\lambda}\right) \tag{10.3}$$

where $l_o = \sin(\theta)$.

Figures 10.2 and 10.3 show how visibilities vary with changes in baseline. Also visible is the change in the visibility measurements due to damping by the wide field factor.

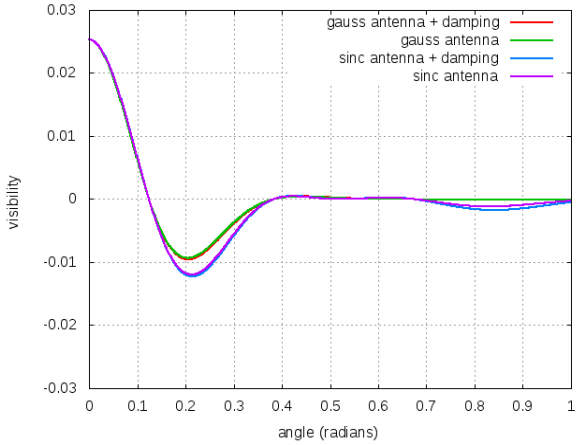

(a) visibility plot for u = 2

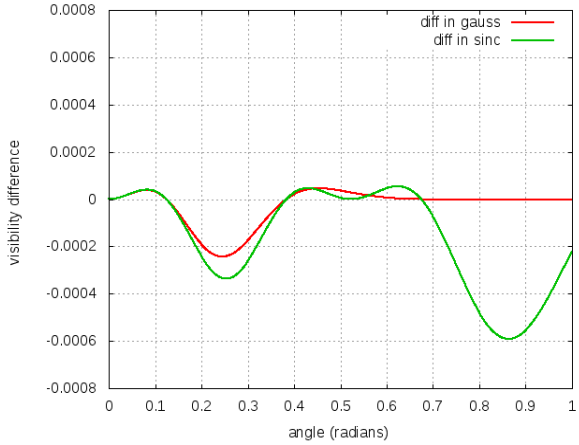

(b) error due to damping for u = 2

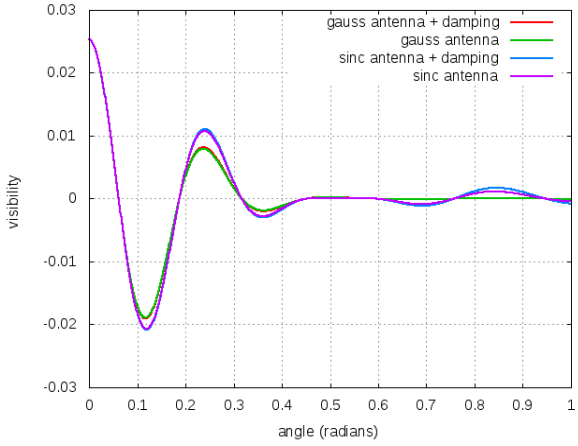

(c) baseline u = 4

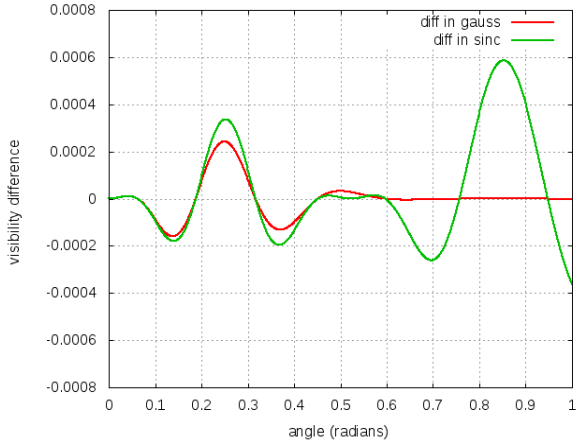

(d) error due to damping for u = 4

Figure 10.2: Column 1: Plot of visibilities for a source moving for one radian, for comparison between two antenna patterns - Gaussian and Sinc functions;
Column 2: Plot of the difference of visibilities with and without damping factor for comparison between the two antenna patterns.

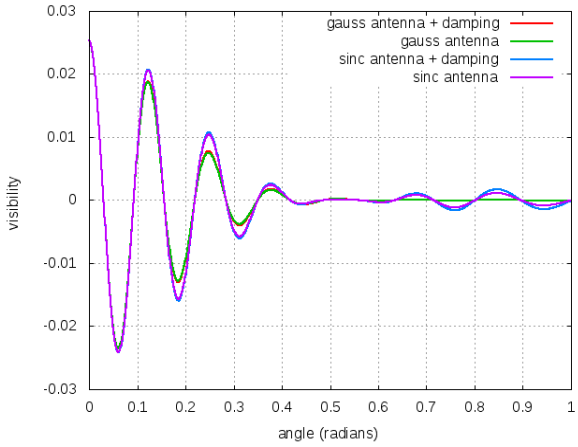

(a) baseline u = 8

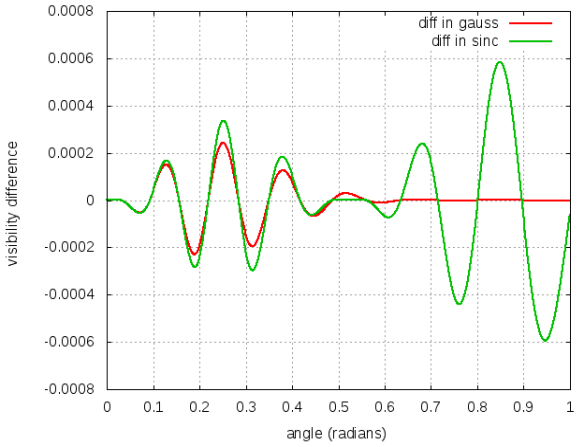

(b) error due to damping for u = 8

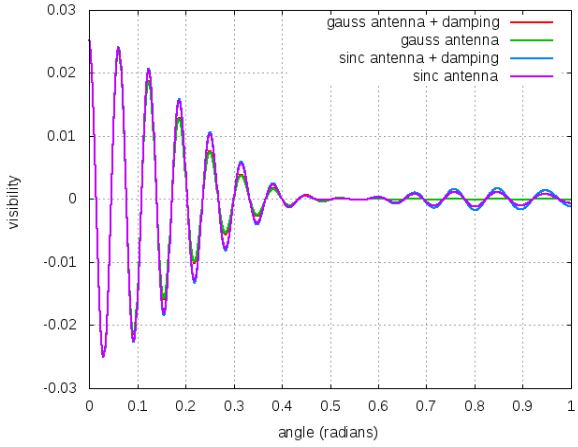

(c) baseline u = 16

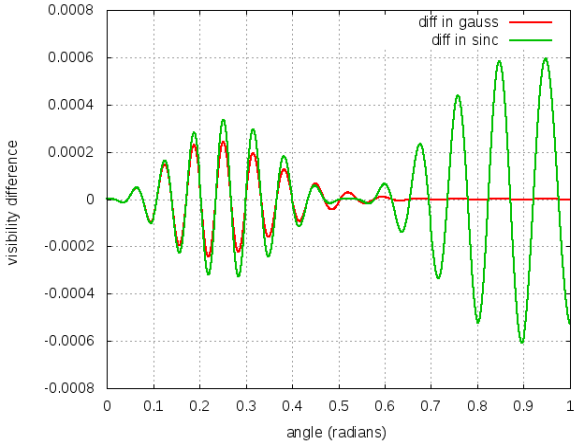

(d) error due to damping for u = 16

Figure 10.3: Column 1: Plot of visibilities for a source moving for one radian, for comparison between two antenna patterns - Gaussian and Sinc functions;
Column 2: Plot of the difference of visibilities with and without damping factor for comparison between the two antenna patterns.

Chapter 11

Case Study II: Murchison Widefield Array

Next, we also look at the Murchison Widefield Array (MWA) located in Western Australia. It operates in the frequency range 80–300 MHz. The FoV is large by the standard of astronomical instruments, being on the order of 30 degrees across.

11.1 Design

The antenna comprises four by four regular grid of dual-polarization dipole elements arranged on a 4m x 4m steel mesh ground plane. Each antenna (with its 16 dipoles) is known as a 'tile'. It is the first so-called large-N array, fully cross-correlating signals from 128 such phased tiles.

The core area has 50 antenna tiles uniformly distributed over a 100 metre diameter core, surrounded by 62 tiles which are distributed over a 1.5 km diameter circle. The final 16 tiles have been placed even further out on a 3 km diameter circle to optimize solar imaging performance, and for the highest angular resolution imaging.

11.2 Wide field observations with MWA

These rectangular tiles make the antenna pattern a Sinc function, with the x and y dimensions to be four. We take a baseline value of $u = 10$ and $v = 10$ and plot

the two dimensional visibilities.

The antenna pattern was taken as

$$A_{sinc} = sinc^2\left(\frac{\pi l_o B_x}{\lambda}\right) sinc^2\left(\frac{\pi m_o B_y}{\lambda}\right) \tag{11.1}$$

where $l_o = \sin\theta$ and $m_o = \sin\phi$.

Figure 11.1a and 11.1b show visibility values without and with damping. To see the errors, we plot the difference plot as in Figure 11.1c.

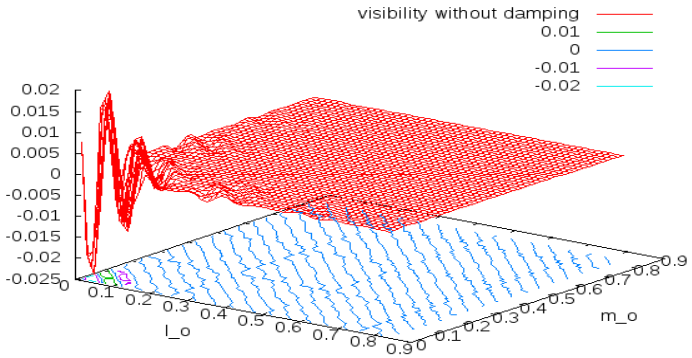

(a) Visibility without Damping

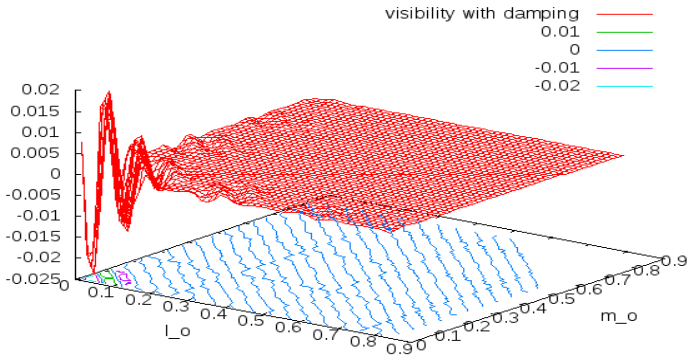

(b) Visibility with Damping

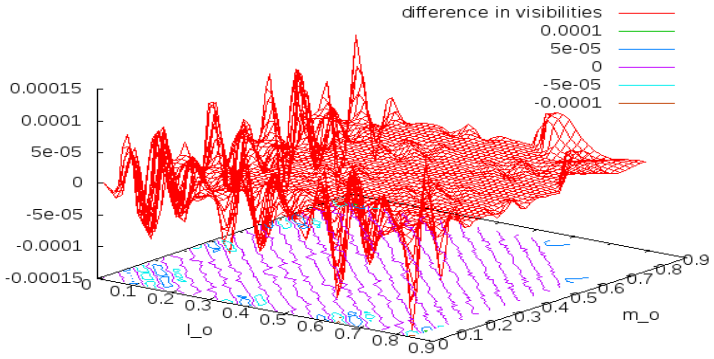

(c) Difference in visibilities with and without Damping

Figure 11.1: Two dimensional visibility plots for MWA using Sinc function as the antenna pattern

Chapter 12

Conclusions

We have looked at the van Cittert Zernike theorem in both the narrow and the wide FoV limit.

For the plots of visibility versus angle, we kept the antenna fixed and move the source from this position to a wide angle. We see that while the Gaussian antenna response decays at higher angles, the Sinc function induces sidelobes.

We correspondingly plot the difference between the visibilities with and without taking into consideration the damping factor. For the Gaussian case, this difference fluctuates to a maximum of about 0.2%, by the time it reaches the large angles, the difference goes to zero since there is no detection of the source. For the Sinc case however, after initial fluctuations comparable to the Gaussian functions, the difference starts to increase when the sidelobes kick in. With increase in baseline, we see increase in fringe oscillations.

For the MWA case, we plot the two dimensional visibility, along with the difference plot. Again, the difference is less than 1%.

For the spherical basis, similar plots can be made. Then the first step would be to calibrate both the methods. This is being carried out presently, the difficulty is to take into account numerical issues that come into the picture due to functions like the spherical harmonics and integration techniques employed.

Once the calibration is done, we can move on imaging, thus exploiting the full benefits of the easier solution in spherical basis.

Bibliography

[1] T. D. Carozzi, arxiv: 1504.04485v2 21 april 2015

[2] T. D. Carozzi and G. Woan, arxiv: 0812.0141v2 19 jan 2009

[3] A Thompson et al, Interferometry and Synthesis in Radio Astronomy

[4] Giant Meterwave Radio Telescope (GMRT) gmrt.ncra.tifr.res.in

[5] National Radio Astronomy Observatory (NRAO) Essential Radio Astronomy.

[6] Tools of radio astronomy, Thomas L Wilson, Springer Publications

[7] David Attwood, Soft X-Rays and extreme ultraviolet radiation.

[8] An introduction to Radio Astronomy second edition, Bernard F. Burke and Francis Graham-Smith, Publisher: Cambridge University Press

[9] Radio Astronomy (2nd edition), John D. Kraus

[10] Ryle, M., A New Radio Interferometer and Its Application to the Observation of Weak Radio Stars, Proc. R. SOC. A , 211,351-375, 1952.

[11] NRAO - Green bank Telescope https://science.nrao.edu/facilities/gbt

[12] NRAO Very Large Array http://www.vla.nrao.edu/

[13] Landon et al 2009, arxiv: 0912.0204

[14] Swarup G. et al., Large Steerable Radio Telescope at Ootacamund, India., Nature Physical Science, Vol. 230, Apr, (1971)